Int. J. Electrochem. Sci., 13 **(2018)** 7265 – 7281, doi: 10.20964/2018.08.38

International Journal of
ELECTROCHEMICAL
SCIENCE
www.electrochemsci.org

Influence of Micro-arc Oxidation Coatings on Corrosion Performances of AZ80 cast alloy

Yuna Xue[1,3,*], *Xin Pang*[2,*], *Bailing Jiang*[1], *Hamid Jahed*[3]

[1] School of Materials Science and Engineering, Xi'an University of Technology, No.5 Jinhua South Road, Xi'an 710048, China
[2] CanmetMATERIALS, Natural Resources Canada, 183 Longwood Road South, Hamilton, ON L8P 0A5, Canada
[3] Department of Mechanical & Mechatronics Engineering, University of Waterloo, 200 University Avenue West, Waterloo, ON N2L 3G1, Canada
[*] E-mail: xynlina@gmail.com, xin.pang@canada.ca

Received: 27 April 2018 / *Accepted:* 31 May 2018 / *Published:* 5 July 2018

To enhance the corrosion performance of cast AZ80 alloy, micro-arc oxidation (MAO) coating was synthesized at various processing current densities in a basic silicate-fluoride solution. The microstructure, composition, corrosion performance and Mott-Schottky characteristics of MAO coatings at different processing current densities were investigated using various microscopic characterization and electrochemical methods. It was found that a thinner (5.04 μm) MAO coating produced at the low processing current density obtained a more uniform and smaller discharge pores morphology and higher fluoride content compared to the other coatings produced at higher current densities. The open-circuit potential, corrosion current density and polarization resistance values of this coating were -1.28 V vs. Ag/AgCl electrode, 0.00589 $\mu A/cm^2$ and 1.53×10^6 $\Omega\cdot cm^2$ in 3.5 wt.% NaCl, respectively. After the Mott-Schottky test, the analysis of the coating showed that the uncoated and MAO coated AZ80 alloy exhibited p-type semiconductor characteristics. For the MAO coated specimens, the coating synthesized at the lower applied current density showed lower acceptor concentration and highly negative flat band potential. These features are associated with the reduced reactivity and improved corrosion resistance of this new MAO coating.

Keywords: Micro-arc oxidation; electrochemical kinetic parameters; Semi-conducing property; AZ80 cast alloy

1. INTRODUCTION

As the lightest structural metal, Mg and its alloys play an increasingly important role in industrial applications due to their excellent strength-to-weight ratio, good machinability, good

electromagnetic shielding characteristics and good recycling ability [1,2]. However, its high susceptibility to corrosion is a significant limitation for many applications [1–5].

Coating is the most widely used method for enhancing the corrosion stability of magnesium alloys. Ceramic coatings block the electric contact between the substrate and the external solution. Among the many different types of coatings [6], micro-arc oxidation (MAO) is a promising surface preparation method that was investigated in 2000 [1]. MAO process can produce a thick, hard and highly corrosion resistant ceramic-like oxide coating on a magnesium alloy. Due to the barrier effect of the MAO coating immersed in a corrosive environment, the transmission of electrons and ions at the electrode and solution interface will be suppressed [7–10]. Many factors affect the formation of the MAO coating. For example, Lu et al. [11] investigated the effects of the discharge intensity on the coating growth direction and the MAO coating formation kinetics and demonstrated that coating at high intensity grows rapidly inward while low intensity enables the outward growth at a low speed. In the same electrolyte, arc discharge intensity is related to the current density of the power output, and the current density plays a significant role in the electrochemical processes. Srinivasan et al. [12] have revealed the microstructure and corrosion performance of the AM50 Mg alloy with plasma electrolytic oxidation (PEO) coating formed at various current densities in a silicate solution. Meanwhile, Liang et al. [13] have investigated the effect of variation of the applied current wave forms on the MAO coated AM60B in silicate electrolytes using a high power bi-polar pulsed electrical source.

The magnesium alloy with MAO coatings fabricated using different processing current densities exhibited different electrochemical behaviors compared to the bare substrate [8,12], especially for the electrochemical properties and semi-conducting behavior of the MAO coating [14,15]. The effects of this processing parameter (current density) on the electron transfer and capacitance variation during the electrochemical processing have not been investigated comprehensively, and the link between the Mott-Schottky electronic characteristics and corrosion properties of MAO coated Mg alloy is also not well established [16–18]. Hence, determination of the semi-conducting characteristics of the MAO coating can help to better understand their corrosion resistance. The primary objective of the present study is to investigate the effects of the processing current density parameter on the electrochemical corrosion performance and semi-conducting characteristics of the MAO coated cast AZ80 magnesium. The MAO process was carried out at three different current densities to produce MAO coatings on the cast AZ80 Mg alloy substrate and the surface structures and morphologies of treated and untreated samples were analyzed. Additionally, the corrosion and semi-conducting performance of these MAO coatings were investigated by advanced electrochemical corrosion tests and the Mott-Schottky (M-S) plots, thereby yielding the values of the corrosion kinetics parameters, flat band potential and donor concentration.

2. EXPERIMENTAL

2.1 MAO coating preparation

The substrate used in this work was the AZ80 cast magnesium alloy consisting of Al 8.4 wt%, Zn 0.48 wt%, Mn 0.2 wt%, Si 0.026 wt%, Cu 0.0026 wt%, and Mg balance. The samples were

mechanically cut into the flat coupons with dimensions of 50 mm ×25 mm ×5 mm from a thick plate of the AZ80 Mg alloy. All specimens were mechanically polished to 1200 grit, cleaned with acetone and distilled water, blow dried at room temperature, and finally placed in a dry tank in reserve.

The MAO process was performed using the equipment obtained from Xi'an University of Technology using a single pulse voltage mode, and the output power was modulated by a constant current. The MAO electrolyte consisted of 5g/L of Na_2SiO_3, 8g/L of KF and 10g/L of KOH in distilled water with the pH of 13. During the MAO fabrication process, the anode was served by the uncoated and coated samples and the cathode was served by a stainless steel. MAO coatings were synthesized at three different processing current densities, i.e., 34 mA/cm^2, 68 mA/cm^2 and 102 mA/cm^2 (with samples marked P1, P2 and P3, respectively) for 5 minutes at a constant pulse width of 80 μs. The temperature of the prepared solution using a water cooling system was kept at the room temperature

2.2 Surface characterization

The topological and cross-sectional morphologies of MAO coatings obtained under different current densities were analyzed using a Philips XL30-SFEG scanning electron microscope (SEM), and the chemical composition of the coatings was measured by energy dispersive X-ray spectrometer (EDS) in the SEM instrument. The phase structure was investigated by X-ray diffraction (XRD) using Cu-Kα radiation with a Bruker-D8 Discover equipped with advanced 2D-detector.

2.3 Electrochemical evaluation

The performance of the MAO coated and uncoated AZ80 samples were evaluated in a 3.5 wt.% NaCl corrosive solution using the three-electrode setup by a potentiostat/galvanostat electrochemical system (Solartron SI 1287 and 1255B) with CorrWare. The typical three-electrode setup was adopted, which includes Ag/AgCl (saturated with KCl) as the reference electrode, and a platinum mesh as the counter electrode. The bare or MAO coated AZ80 specimens exposing the area of 1 cm^2 were used as the working electrode. These techniques used in the tests are listed below.

(1) Open-circuit potential (OCP) measurements

The OCP vs. time (t) curve was used as a measure of the spontaneity of the reaction and a rough indication of tendency to corrode for the coated and uncoated samples. After the samples were immersed in the corrosive medium, OCP was measured for 0.5 h, during which time the potential settled to a steady state.

(2) Electrochemical impedance spectroscopy (EIS)

After the OCP test, EIS data were obtained at the frequencies from 100 kHz to 10 mHz with the perturbation signal amplitude of 10 mV. The ZSimpWin software was used for the EIS data modeling and curve-fitting.

(3) Potentiodynamic polarization (PDP)

Potentiodynamic polarization tests were conducted to evaluate the electrochemical performances of the samples at the sweep rate of 1 mV/s in the potential range from -0.2 V to 0.5 V (vs. OCP), and

Tafel plots were obtained from the tests.

(4) M-S analysis

The Mott-Schottky test was conducted to determine the semi-conducting characteristics of the uncoated and MAO coated AZ80 samples. This test mainly involves the measurement of the capacitance C as a function of the applied potential (E). The capacitance values were obtained at different controlled potentials in the range between -1.2 V and 0.2 V with the interval of 50 mV at 1 kHz. The M-S data is shown in a plot of (C^{-2}) vs. E.

All electrochemical tests were carried out by repeating the tests three times to ensure reproducibility.

3. RESULTS AND DISCUSSION

To evaluate the influence of processing current density on the performances of MAO coated cast AZ80, the morphology, composition, corrosion and semi-conducting properties of MAO coating were systemically analyzed.

3.1 Surface characterization

The surface and cross-sectional morphologies, element composition and particles distribution of the MAO coatings were analyzed with SEM and EDS. The surface morphologies of MAO coated AZ80 specimens synthesized at various processing current densities are displayed in Figure 1. For the sample P1 prepared at 34 mA/cm^2, the pores are small and uniform. With the higher processing current densities, some large oxide particles and micro-cracks were obtained which were randomly distributed on the surface, and the sizes of the pores are larger than those of sample P1. Sample P3 treated at 102 mA/cm^2 showed large oxide chunks integrated with each other, which is due to the highest energy input and large spark sizes during the MAO process [19].

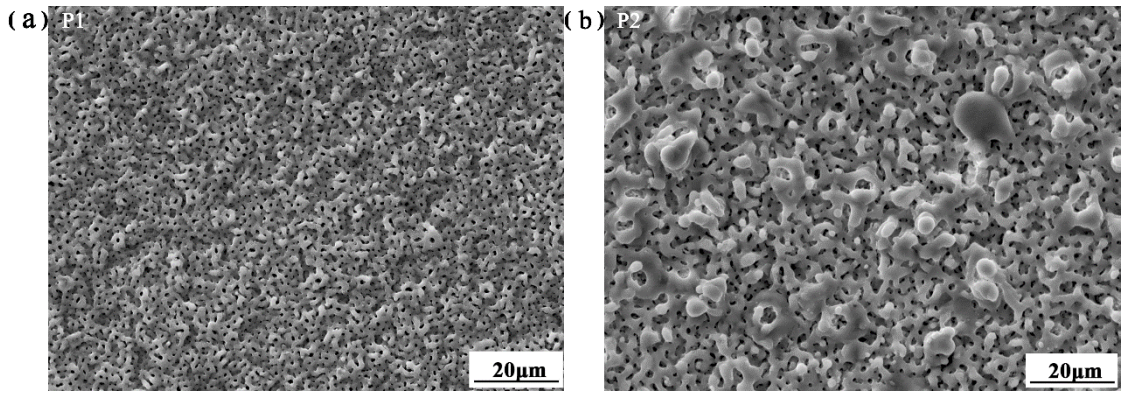

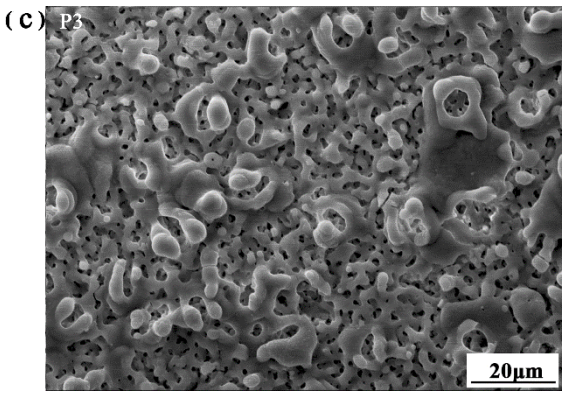

Figure 1. Surface micrographs of MAO coated AZ80 obtained at various current densities: (a) P1 -34 mA/cm^2, (b) P2 -68 mA/cm^2 and (c) P3 -102 mA/cm^2

The chemical compositions (at. %) of the MAO coatings measured by EDS are shown in Table 1. The results of semi-quantitative EDS analysis show that the MAO coating mainly consisted of Mg, O, Si, Al and F elements, and elemental composition of the MAO coatings obtained under different processing current densities are almost identical. The fraction of F in the MAO coating decreased with the increased current density, while those of O and Al increased, and a significant difference in Si content was observed for all coatings.

Table 1. EDS analysis of the atomic concentration of elements in the MAO coatings

Samples	Atomic concentration (%)				
	Mg	O	Si	Al	F
P1(34 mA/cm^2)	46.43	38.08	6.61	3.98	5.01
P2(68 mA/cm^2)	46.11	39.50	6.48	4.25	4.10
P3(102 mA/cm^2)	44.85	41.38	6.54	4.69	3.12

Figure 2 displays the cross-sectional morphology and the corresponding elemental distribution characteristics of the MAO coated AZ80 Mg samples (P1, P2 and P3). The average thicknesses for the P1, P2 and P3 specimens are 5.04, 13.41 and 18.74 μm, respectively, and the MAO coating formed at 102 mA/cm^2 was 3.5 times thicker than the coating produced at 34 mA/cm^2. With the increase of the processing current density, the coatings showed a more wavy-jagged coating/substrate interface with some pores near the interface, which is most likely due to the increasing speed of the inward growth of the coating and gas bubbles released by micro-arc discharge channels in the beginning of MAO processing [20]. Dense and uniform ceramic coatings were formed at the low applied current density, while the coating prepared at the intermediate parameter level (P2) showed a higher porosity and greater degree of micro-cracks than that for P1. In high processing current density operations, the pore channels and micro-cracks on the surface are most likely to be interconnected and reach the substrate. The elemental distribution analysis results (Figure 2) show that both Mg and O were uniformly distributed in all coatings. By contrast, Si is mainly concentrated on the coating surface, and the F

element which represents the protective MgF_2 phase (Fig. 3) is enriched near the substrate and Al is mainly distributed on the top and bottom of the coating.

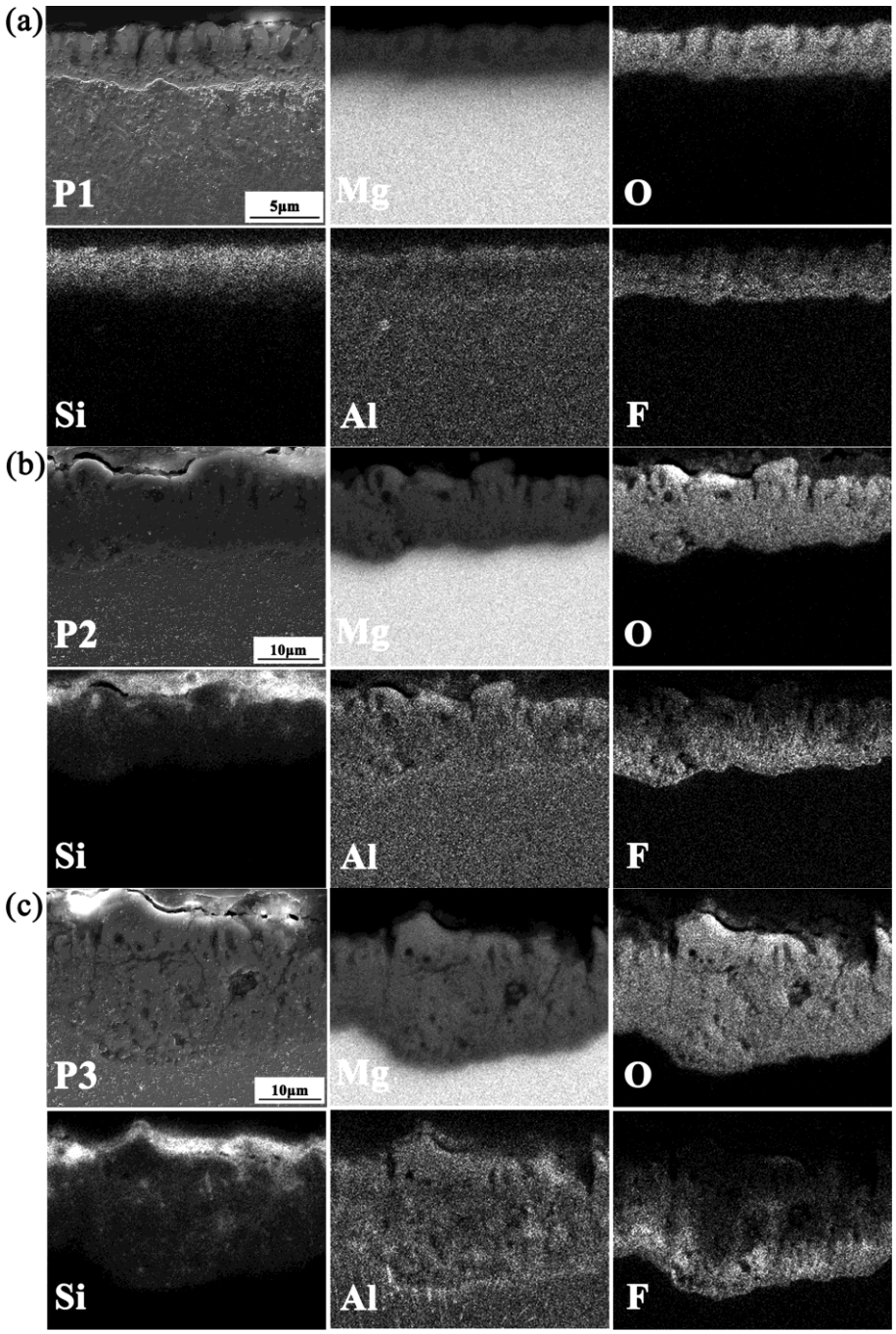

Figure 2. Cross-section micrographs and corresponding EDS maps of MAO coatings (a) P1 at 34 mA/cm^2, (b) P2 at 68 mA/cm^2 and (c) P3 at 102 mA/cm^2

Based on the coating morphology analysis discussed above, the control of the processing current density is very important for the quality of the MAO coating. The current density can directly regulate the characteristics of spark discharge and microstructure of the coating. Generally, high

current density increases the intensity of the spark discharge associated with a high pulse energy, leading to the formation of rough and porous microstructure of the MAO coating. In contrast, low current density contributes to the formation of the microstructure of fine holes and less porous coating[19,21,22].

Figure 3 shows the XRD results of the uncoated and MAO coated cast AZ80 alloy. As seen in this figure, the uncoated AZ80 sample is composed of mainly Mg and $Mg_{17}Al_{12}$, an electrochemically noble phase in the base alloy. MAO coatings formed at different processing current densities have the same phases in the coating: β-$Mg_{17}Al_{12}$, MgO, Mg_2SiO_4, and MgF_2. Some complex silicate compounds, namely, $Mg_3Al_2(SiO_4)_3$ and $Mg_xF_y(SiO_4)_z$, are present as well. At the same time, the coefficients x and y depends on the Mg and F contents, implying that the content of MgF_2 in MAO coating can drift with the current density processing parameter, as reported by Liang et al. [13]. It can be seen from the results of elemental analysis (Table 1) that for the P1 sample prepared at the lower processing current density, the coefficients x and y are high due to the relatively high content of F and Mg in the MAO coating. Comparison of the F element content values shows that the lower processing current density resulted in a higher content of the protective magnesium fluoride compound.

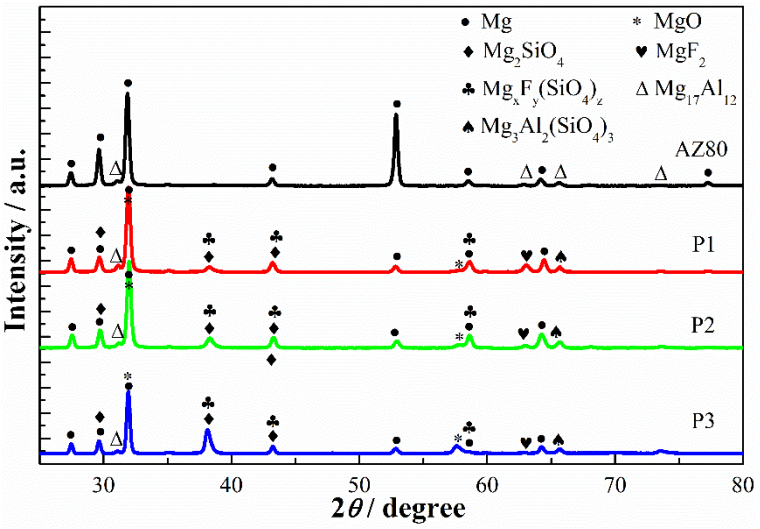

Figure 3. XRD analysis data for cast AZ80 alloy samples P1, P2 and P3 with MAO coatings

3.2 Corrosion performances

3.2.1 OCP measurement

The variation of OCP of the samples with immersion time in the salt solution was recorded. The OCP represents the thermodynamic propensity of an electrode to participate in the corrosive environment through electrochemical reactions. The higher (more noble) value of the OCP of an electrode indicates a lower inclination to corrode under corrosive conditions [14,23,24]. Figure 4 shows the OCP vs. time curves of the substrate AZ80 and the P1, P2, P3 samples after 30 min immersion.

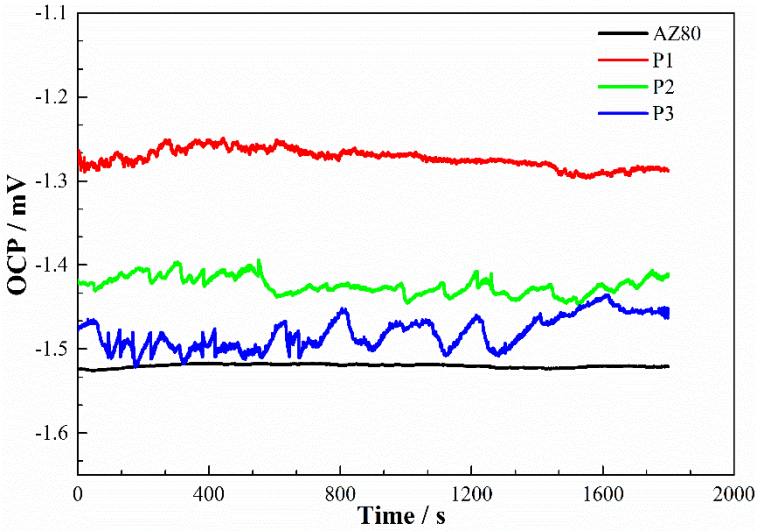

Figure 4. OCP curves of the MAO coated and uncoated AZ80 samples immersed in 3.5 wt.% NaCl solution for 30 min

During the immersion, the OCP shifts to the noble or negative direction depending on the surface performance of the electrode and the rate of charge transfer at which the equilibrium of the involved ionic species is established [14], and thereby gradually reaches a stable and saturated state. Figure 4 showed that the OCP of the substrate AZ80 exhibited a stable potential of -1.52 V. It can be seen that the OCP curves of the MAO coated AZ80 (P1, P2 and P3 specimens) at different processing current densities shifted obviously towards the more positive direction compared to that of the uncoated AZ80. The average OCP values for the P1, P2 and P3 samples were -1.28 V, -1.41 V and -1.45 V, respectively, indicating that the MAO coated AZ80 samples are more thermodynamically stable than the bare AZ80 substrate when immersed in the 3.5 wt.% NaCl environment.

As shown in Fig. 5, the fluctuation of the OCP of the MAO coating mainly depends on the surface features of the samples including their microstructure and chemical composition and the compactness of the barrier coating formed at the substrate/coating interface[24–26]. Compared to the MAO coating formed at a lower current density, the coating synthesized at a higher processing current density has more defects such as large solid particles (mainly MgO phase), large micro-pores and micro-cracks on its surface. These structural defects enlarged the effective surface area and allowed the aggressive anions (e.g., Cl^-) in the corrosive environment to readily infiltrate and reach the substrate/coating interface; the fluctuating open current potential can reflect the non-uniform surface structure [10,22]. Furthermore, the OCP of the test samples showed the order of P1＞P2＞P3＞AZ80, indicating the decreasing tendency for corrosion of MAO coated AZ80 samples from P3 to P2 and P1.

3.2.3 EIS analysis

The EIS has been an essential semi-quantitative for the evaluation and measurement of the polarization resistance for the prediction of the corrosion protective performance of the surface coatings on metals in corrosive environments [27,28]. In this work, the polarization characteristics of

the uncoated and MAO coated AZ80 samples (P1, P2 and P3) were examined by EIS at OCP after immersion for 30 min in 3.5 wt.% NaCl corrosive environment. The results of simulation and experiments for Bode impedance (Frequency vs.$|Z|$) and phase angle (Frequency vs. theta) plots are shown in Figure 6.

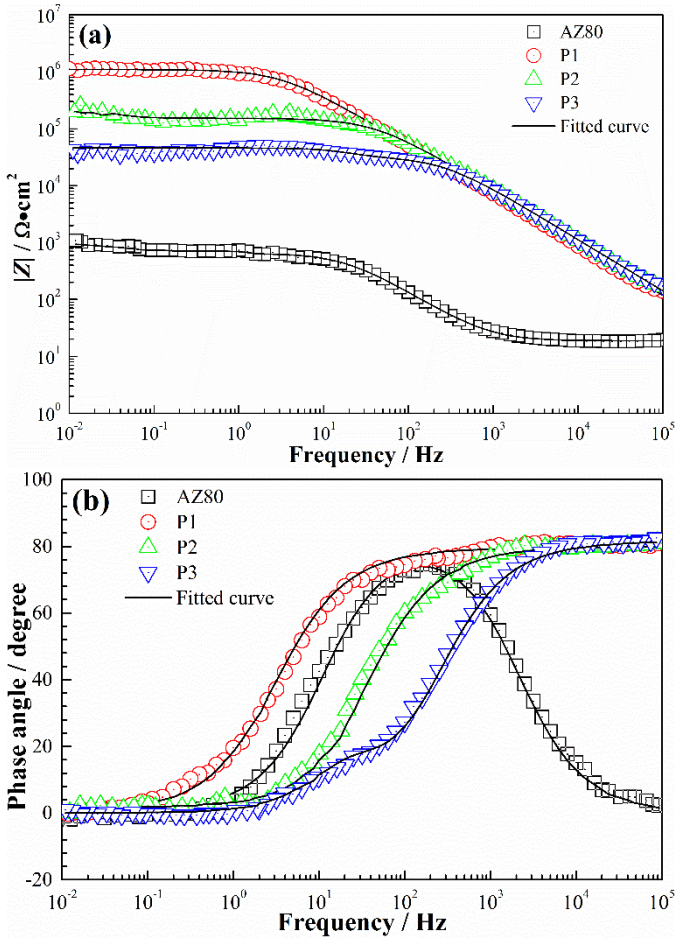

Figure 6. Experimental (a) Bode impedance and (b) phase angle vs. frequency curves after fitting for MAO coated and uncoated AZ80 samples

Figure 7 shows the fitted equivalent circuit models for the EIS data that use various circuit elements including resistors, capacitors and parallel combinations for bare AZ80 substrate and coated samples P1, P2, and P3. For both uncoated and coated AZ80 samples, when the electrical double-layer was established after immersion in the corrosive electrolyte, all circuit elements represent the electron transfer state of these electrode system [29,30]. In Figure 7, R_s represents the electrolyte resistance between the reference and working electrodes. The electrical double-layer is characterized by the charge transfer resistance R_{ct} in parallel with the double-layer capacitance Q_{ct}. The MAO coating layer is represented as the coating resistance R_{mf} in parallel with the coating capacitance Q_{mf}. The results of the curve-fitting analyses are listed in

Table 2.

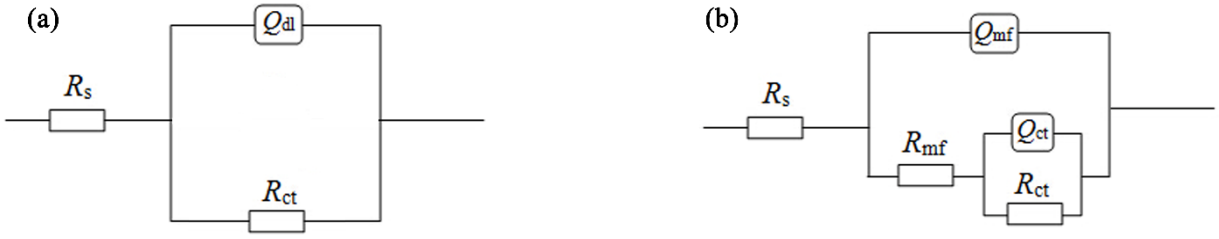

Figure 7. Equivalent circuit of the (a) uncoated and (b) MAO coated AZ80 samples

Table 2. Fitted values of the equivalent circuit elements for untreated and MAO treated specimens tested in 3.5 wt.% NaCl solution

Specimen	Q_{dl} ($uF/cm^{-2}\cdot s^{1-n}$)	n	R_{ct} ($\Omega\cdot cm^2$)				R_p ($\Omega\cdot cm^2$)
AZ80	8.92	0.9305	3.147×10^3				3.147×10^3
Specimen	Q_{mf} ($uF/cm^{-2}\cdot s^{1-n}$)	n	R_{mf} ($\Omega\cdot cm^2$)	Q_{dl} ($uF/cm^{-2}\cdot s^{1-n}$)	n	R_{ct} ($\Omega\cdot cm^2$)	R_p ($\Omega\cdot cm^2$)
P1	0.1028	0.8592	4.279×10^5	0.0401	0.8828	1.101×10^6	1.5289×10^6
P2	0.2031	0.7450	3.377×10^4	0.0501	0.8880	1.538×10^5	1.8757×10^5
P3	0.6467	0.6213	1.338×10^4	0.0647	0.9048	3.260×10^4	4.5980×10^4

It can be observed from the EIS results that the polarization resistance R_p (R_p=R_{ct} for AZ80 base alloy, R_p=R_{mf}+R_{ct} for P1, P2 and P3) of the magnesium alloy electrodes clearly increased by two orders of magnitude due to the formation of the MAO coating. MAO coated AZ80 substrate greatly increased the charge transfer resistance R_{ct} and coating resistance R_{mf}. The coating structure and chemical composition dictate the EIS behavior and charge transfer mechanism [8]. For all samples, the response in the low frequency range of the electrochemical system characterizes the charge transfer process. Compared to the bare AZ80 substrate, the value of the phase angle of the MAO coated samples are higher in the high frequency range reflecting the MAO coating layer properties [31]. For all coated specimens, the values of R_{ct} are significantly higher than the corresponding R_{mf} values, suggesting that it is the compactness of the inner coating on the substrate that offers the main corrosion resistance. Thus, the charge transfer process is mainly controlled by electrochemical kinetics as represented by R_{ct}. The overall R_p values decreased in the order of P1＞P2＞P3＞AZ80, indicating that the P1 coating obtained at the lowest current density contributed the highest polarization resistance among the MAO treated specimens because of its compact structure (low porosity and no cracks) and high fluoride content (note that MgF_2 is more stable than MgO). These results are similar to the findings of Liang [32]. The coating formed at a higher current density level (P3) has a low value of R_p, which can be attributed to the large pores and conducting pore channels in the coating (as shown in Sec. 3.1). The leakage of the electrolyte into the substrate through the micro-cracks and pores in the coating is responsible for the low corrosion resistance of the P3 specimen.

3.2.3 PDP

Figure 8 depicts the PDP curves of the uncoated and MAO coated samples. The corrosion potential E_{corr} which is the potential of zero current from the polarization curves, corrosion current density i_{corr}, and the Tafel constants of anode b_a and cathode b_c are obtained by using the curve-fitting approach in the weak-polarization zone [23]. The fitted values of the corrosion kinetics parameters for MAO coated and uncoated samples are listed in

Table 3.

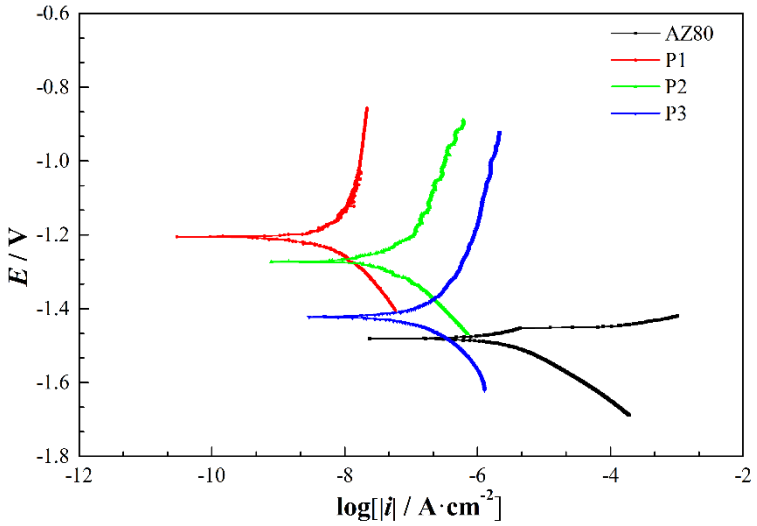

Figure 8. PDP curves obtained for bare AZ80, P1, P2 and P3 specimens in 3.5 wt.% NaCl solution

Table 3. Fitted corrosion kinetics parameters for the bare AZ80, P1, P2 and P3 samples in 3.5 wt.% NaCl

Specimen	E_{corr}(V)	i_{corr}（μA•cm^{-2}）	b_a(mV•dec^{-1})	b_c(mV•dec^{-1})
AZ80	-1.48	2.9	31	115
P1	-1.21	5.89×10^{-3}	183	133
P2	-1.27	3.90×10^{-2}	152	128
P3	-1.42	1.55×10^{-1}	146	119

It can be seen from the fitted corrosion kinetics parameters that the untreated bare AZ80 showed the corrosion current density i_{corr} of 2.9 μA/cm^2 with the joint corrosion potential E_{corr} of -1.48 V. The i_{corr} values for all MAO coated samples were smaller by 1-3 orders of magnitude than the bare AZ80. Among the coated samples, the i_{corr} of the MAO coating obtained at the lower current density condition was smaller, indicating a better corrosion resistance and following a trend similar to that observed in the EIS results discussed above. The higher values of the anodic Tafel constants b_a provide the MAO coating with the passivation behavior.

In practice, the enhanced corrosion resistance of the MAO coating depends on the resistance of the coating to the transmission of the ions from the corrosive environment to the coating/substrate interface and the diffusion of the substrate ions, which is determined primarily by the structural, compositional, and morphological properties of the coating and the strength of the bonding between the coating layer and the substrate [33,34]. Consequently, in the present work, the P1 sample shows excellent corrosion resistance due to its lowest coating porosity and highest content of stable barrier oxide compound formed during the low current density coating process.

3.3 Electronic properties of MAO coatings (M-S analysis)

The performances of MAO coating, especially corrosion characteristics such as the charge transfer rate and the permeability of corrosive ions are not only dependent on the morphology, elemental and phase composition of the surface coating but also on its defect density and electronic properties. The electronic properties of the MAO treated and untreated surfaces is best understood using Mott-Schottky analysis [35–38]. In the corrosive medium, the presence of point defects in the coatings makes them show different semiconductor properties. According to the point defect model, the cationic vacancies are electron acceptors resulting in the p-type conduction in the coating, whereas the electron donors include the oxygen vacancies and the metal interstitials leading to the n-type doping [8,21,39–41]. Using the Mott-Schottky theory which describes the performance of the interface between the semiconductor and the electrolyte, the capacitance data (C) of the coating/electrolyte interface under different applied potentials (E) can be analyzed using the following equations (1) & (2):

$$1/C^2 = 2/\varepsilon\varepsilon_0 q N_D \left(E - E_{fb} - kT/e\right) \text{ for n-type semiconductor} \quad (1)$$

$$1/C^2 = -2/\varepsilon\varepsilon_0 q N_A \left(E - E_{fb} - kT/e\right) \text{ for p-type semiconductor} \quad (2)$$

where ε is the relative permittivity (dielectric constant) of the oxide coating (taken as 9.6 for Mg alloys [21]), ε_0 is the vacuum permittivity (8.85×10^{-14} F/cm), q is the elementary charge 1.602×10^{-19} Coulombs (-e for electrons and +e for holes), N_D and N_A are the donor and acceptor concentrations, respectively, E_{fb} is the flat band potential, E is the applied potential, k is the Boltzmann constant (1.38×10^{-23}J/K), and T is the absolute temperature. kT/e (neglect) [14]. This equation reveals a linear C^{-2} vs. E plot, where the intercept with the E-axis shows the value of the flat band potential, and the slope represents the value of the donor or acceptor concentration [16,17].

The Mott-Schottky (M-S) plots obtained for bare AZ80 and MAO coated samples are presented in Figure 9. A linear relationship between C^{-2} and E with a negative slope is found for all tested specimens. This indicates that both uncoated and MAO coated AZ80 samples achieved p-type semiconducting behavior in 3.5 wt.% NaCl corrosive environment. This means that the conductivity of the samples mainly relies on the cationic vacancies in the valence band. Therefore, the active dissolution rate of the MAO treated and untreated samples are mainly influenced by the acceptor concentration N_A of the coating. A more negative E_{fb} and lower N_A make the electrode surface less reactive to the electrolyte anions, as reported elsewhere [8].

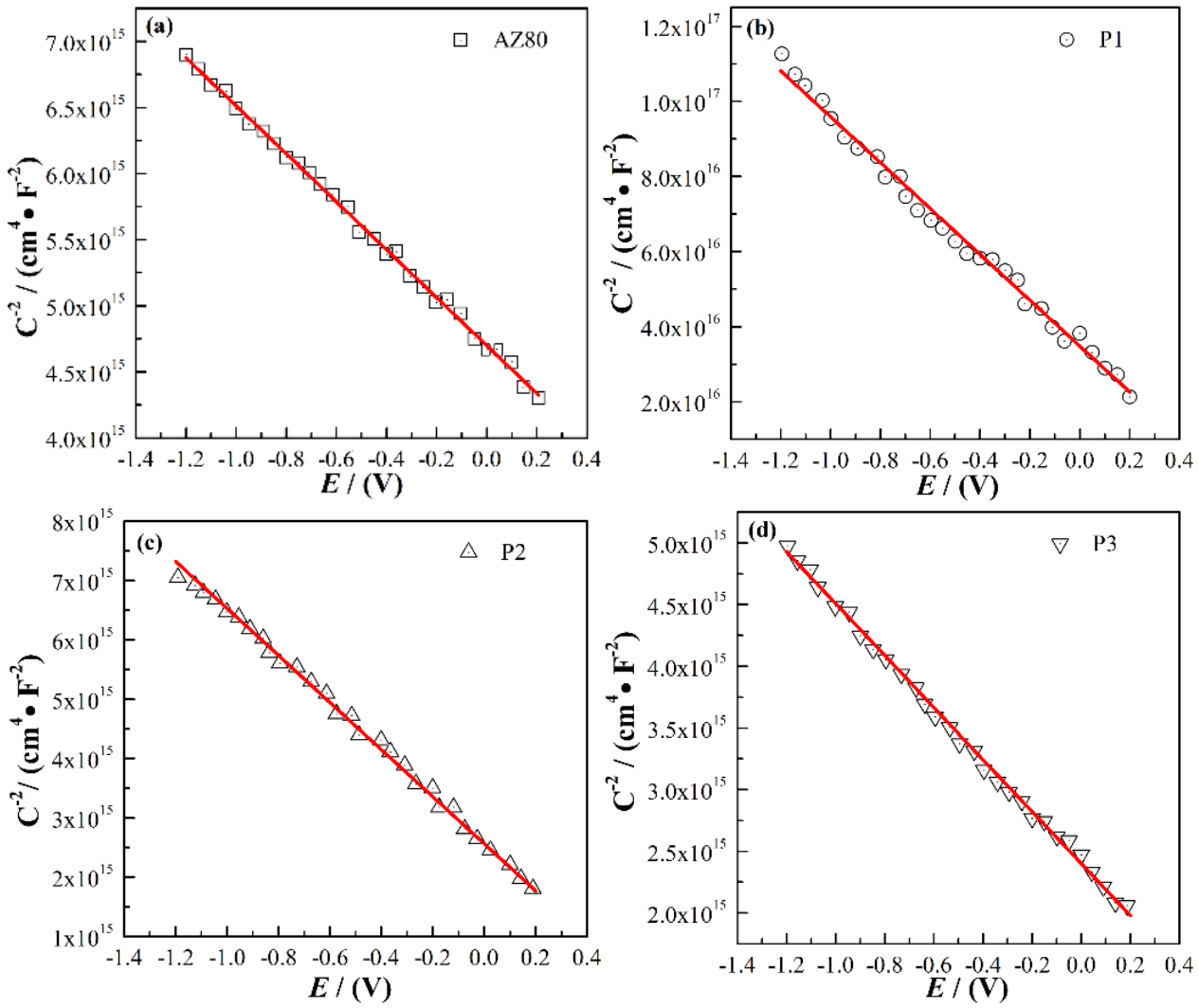

Figure 9. Mott-Schottky plots with fitting curves for the (a) bare AZ80, (b) P1, (c) P2 and (d) P3 samples in 3.5 wt.% NaCl solution

Table 4 displays the values of acceptor concentrations (N_A) and flat band potential (E_{fb}) obtained for the MAO treated and untreated samples. It is shown that the N_A and E_{fb} of bare AZ80 substrate were much higher than those of the MAO coated specimens, and the acceptor density of the different MAO coatings decreased in the order of P3＞P2＞P1. In Cl^- solutions, the surface of the Mg alloy samples are attacked by corrosive Cl^- via the mechanism of penetration and dissolution. This means that the Cl^- migrates or diffuses in the oxide or the metal surface and then penetrates through the oxide and finally destabilizes the surface of the electrode, giving rise to active dissolution of the substrate. A higher acceptor concentrations (N_A) leads to more cationic vacancies enriched on the surface of the electrode, which can hold more Cl^- together by electrostatic attraction, making the electrode less resistant to corrosion. Therefore, the corrosion performance of the magnesium alloy was enhanced significantly by the MAO treatment, due to the formation of stable ceramic MAO coating sintered on the substrate, with the coating obtained at the low processing current density being especially dense and compact. This compact coating effectively prevented the adsorption reaction of

Cl^- into the oxide structure formed on the metal. In summary, the capacitance measurements may be regarded as a useful method for the assessment of the anti-corrosion quality of the MAO coating synthesized on the Mg alloy.

Table 4. Acceptor concentration (N_A) and flat band potential (E_{fb}) values calculated from the Mott-Schottky data of AZ80, P1, P2 and P3 samples

Specimen	$N_A(cm^{-3})$	E_{fb}（V）
AZ80	1.35×10^{16}	2.59
P1	2.39×10^{14}	0.56
P2	3.68×10^{15}	0.65
P3	6.93×10^{15}	1.12

3.4 Charge transfer mechanisms

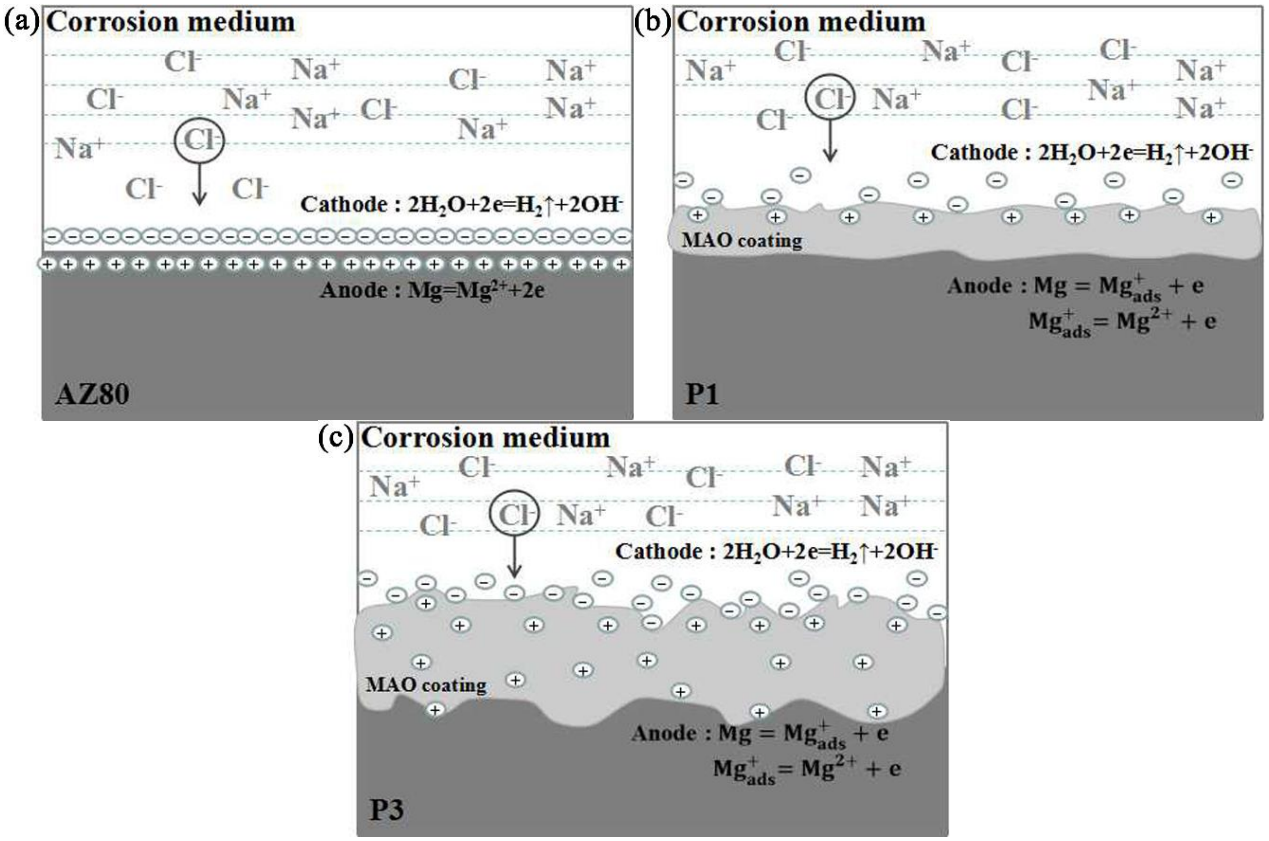

Figure 10. Interface states of (a) bare substrate and MAO treated (b for P1 and c for P3) specimens during the corrosion process in 3.5 wt.% NaCl solution

Electrochemical corrosion of metals is governed by the interfacial charge transfer, and the corrosion kinetics are also related to the ionic migration process in the aqueous solution, as in the case of a diffusion-controlled corrosion process. Figure 10 shows the macroscopic model of interface states for the MAO coated and uncoated AZ80 Mg alloy samples during the corrosion process in 3.5 wt.% NaCl solution. When the metal electrode is exposed to the corrosive medium, the redistribution of the

charge on the metal surface will occur between the interface of the metal surface and corrosive medium. This charge arrangement results in the development of a space charge region near the surface of the samples, due to the difference between the Fermi energy level of the sample surface and the Fermi level (redox potential) of the corrosive environments [14].

As shown by the results discussed in the previous sections, the bare AZ80 substrate has the highest N_A and E_{fb}, and its potential energy level is closer to the conduction band for the more negative OCP. When the AZ80 substrate is exposed to a corrosive medium, its higher concentration of positively charged cationic vacancies may attract more corrosive anions (Cl^-) to its surface as shown in Figure 10(a). The build-up of chloride ions can cause the destruction of the surface and consequently gives rise to the lower resistance to corrosion. Sample P1 has the most uniform and dense MAO coating, and its N_A is the lowest compared to the other coated samples. Its potential energy level is closer to the valence band and is maintained at a relatively stable state during the immersion process (Figure 10(b)). The P3 sample produced at the highest current density has large oxide particles, highest porosity and multiple micro-cracks in its coating and higher N_A and E_{fb} compared to the other two coatings. When the P3 sample was immersed into the 3.5 wt.% NaCl solution, the aggressive Cl^- anions penetrated through the sample surface from the micro-pores and cracks driven by the electrostatic force of cationic vacancies. Due to the weak coating/substrate interface and high content of cationic vacancies in the coating, the corrosive anions (Cl^-) can easily adsorb and penetrate through the MAO coating layer and reach the Mg alloy substrate, and therefore inferior corrosion performances were observed for the sample P3 compared to sample P1. When the alloy begins to corrode, according to the result of the PDP test and the values of the anodic Tafel slope shown in Table 3, the uncoated and MAO coated specimens present different anode reaction and similar cathode reaction mechanisms (Fig. 9). The anodic Tafel slope (b_a) is 31 mV/decade for the AZ80 substrate, which is close to the theoretical Tafel slope value of 59 mV/decade for a two-electron oxidation reaction. For the MAO coated specimens, the anodic Tafel constants are higher and close to the theoretical Tafel slope value of 118 mV/decade for a one-electron oxidation reaction forming the intermediate products of magnesium alloy (Mg_{ads}) [23,42]. All of these results indicated that the MAO coating exhibited a suppressing effect on the anodic reactions of the Mg alloys, and the corrosion resistance depends on the quality of the MAO coating.

4. CONCLUSIONS

Three different current densities were used for the micro-arc oxidation processing of the AZ80 alloy in an alkaline silicate electrolyte. Experimental results have shown that a higher processing current density in the MAO process led to an increased sparking discharge intensity and resulted in a coating having larger oxide particles and micro-pores and more micro-cracks. By contrast, a lower processing current density led to the formation of a fine, uniform, and dense MAO coating on the AZ80 Mg alloy. In particular:

(1) The MAO coating formed at 34 mA/cm^2 showed a lower corrosion current density of 5.89×10^{-3}μA•cm^{-2} and higher polarization resistance of 1.5289×10^6 Ω·cm^2, which is about three orders of magnitude higher than that of the bare substrate AZ80 alloy, demonstrating the excellent corrosion resistance provide by the MAO coating.

(2) Mott-Schottky analysis indicated that the MAO coated and uncoated AZ80 showed p-type semi-conducting behavior. The coating obtained at 34 mA/cm^2 had lower acceptor concentration and flat band potential than the bare base alloy and the other coatings, which were obtained at the higher current densities. These results further confirmed the robust corrosion resistance of the MAO coating.

ACKNOWLEDGEMENTS

This work was financially supported by the Natural Sciences and Engineering Research Council of Canada, the Automotive Partnership Canada (APC) program (Grant No. APCPJ 459269-13). The technical support of Chao Shi of CanmetMATERIALS, Natural Resources Canada, Dr. Sugrib Shaha and Jie Wang of the University of Waterloo during the course of this work is gratefully acknowledged.

References

1. J. Liang, P.B. Srinivasan, C. Blawert and W. Dietzel, *Electrochim. Acta*, 55 (2010) 6802.
2. C. Liu, J. Liang, J. Zhou, Q. Li and L. Wang, *Appl. Surf. Sci*., 382 (2016) 47.
3. Y. Song, K. Dong, D. Shan and E.H. Han, *J. Magnesium Allo*ys, 1 (2013) 82.
4. S. Feliu and I. Llorente, *Appl. Surf. Sci*., 347 (2015) 736.
5. C.E. Barchiche, D. Veys-Renaux and E. Rocca, *Surf. Coat. Technol*., 205 (2011) 4243.
6. J.E. Gray and B. Luan, *J. Alloys Compd*., 336 (2002) 88.
7. Y. Gu, H. Ma, W. Yue, B. Tian, L. Chen and D. Mao, *J. Alloys Compd*., 681 (2016) 120.
8. H. Duan, C. Yan and F. Wang, *Electrochim. Acta*, 52 (2007) 3785.
9. O. Khaselev, D. Weiss and J. Yahalom, *Corros. Sci*., 43 (2001) 1295.
10. V. Birss, S. Xia, R. Yue and R.G. Rateick, *J. Electrochem. Soc.*, 151 (2004) B1.
11. X. Lu, C. Blawert, K.U. Kainer and M.L. Zheludkevich, *Electrochim. Acta*, 196 (2016) 680.
12. P. B. Srinivasan, J. Liang, C. Blawert, M. Störmer and W. Dietzel, *Appl. Surf. Sci*., 255 (2009) 4212.
13. J. Liang, L. Hu and J. Hao, *Appl. Surf. Sci.*, 253 (2007) 6939.
14. K. Venkateswarlu, N. Rameshbabu, D. Sreekanth, M. Sandhyarani, A.C. Bose, V. Muthupandi and S. Subramanian, *Electrochim. Acta*, 105 (2013) 468.
15. A. Ghasemi, V.S. Raja, C. Blawert, W. Dietzel and K.U. Kainer, *Surf. Coat. Technol.*, 204 (2010) 1469.
16. V. Ezhilselvi, J. Nithin, J.N. Balaraju and S. Subramanian, *Surf. Coat. Technol.*, 288 (2016) 221.
17 M. Metikoš-Huković, S. Omanović and A. Jukić, *Electrochim. Acta*, 45 (1999) 977.
18. R. D. Gryse, W.P. Gomes, F. Cardon and J. Vennik *J. Electrochem. Soc.*, 122 (1975) 711.
19. Y. Yue and W. Hua, *T. Nonferr. Metal. Soc.*, 20 (2010) 1.
20. Y. Mori, A. Koshi, J. Liao, H. Asoh and S. Ono, *Corros. Sci.*, 88 (2014) 254.
21. M. S. Joni, A. Fattah-alhosseini, *J. Alloys Compd*., 661 (2016) 237.
22. H. Duan, K. Du, C. Yan and F. Wang, *Electrochim. Acta*, 51 (2006) 2898.
23. R. Wang, S. Luo, M. Liu and Y. Xue, *Corros. Sci.*, 85 (2014) 270.
24. Z. Yao, Z. Jiang, X. Sun, S. Xin and Z. Wu, *Mater. Chem. Phys.*, 92 (2005) 408.

25. A. Bai, P. Chuang and C. Hu, *Mater. Chem. Phys.*, 82 (2003) 93.
26. H. Duan, C. Yan and F. Wang, *Electrochim. Acta*, 52 (2007) 5002.
27. V. Barranco, S. Feliu Jr., S. Feliu, *Corros. Sci.*, 46 (2004) 2203.
28. S. Feliu Jr., C. Maffiotte, A. Samaniego, J.C. Galván and V. Barranco, *Electrochim. Acta*, 56 (2011) 4554.
29. S. Sathiyanarayanan, S.S. Azim and G. Venkatachari, *Appl. Surf. Sci.*, 253 (2006) 2113.
30. A. Ghasemi, V.S. Raja, C. Blawert, W. Dietzel and K.U. Kainer, *Surf. Coat. Technol*., 202 (2008) 3513.
31. S.J. Xia, R. Yue, R.G. Rateick Jr and V.I. Birss, *J. Electrochem. Soc.*, 151 (2004) B179.
32. J. Liang, B. Guo, J. Tian, H. Liu, J. Zhou and T. Xu, *Appl. Surf. Sci.*, 252 (2005) 345.
33. X. Zhang, Z. Jiang, Z. Yao and Z. Wu, *Corros. Sci.*, 52 (2010) 3465.
34. M. Shokouhfar, C. Dehghanian, M. Montazeri and A. Baradaran, *Appl. Surf. Sci.*, 258 (2012) 2416.
35. A. Fattah-alhosseini and H. Asgari, *Arab. J. Sci. Eng*., 41 (2016) 169.
36 M.C.L. de Oliveira, V.S.M. Pereira, O.V. Correa, N.B. de Lima and R.A. Antunes, *Corros. Sci.*, 69 (2013) 311.
37. L. Hamadou, A. Kadri and N. Benbrahim, *Appl. Surf. Sci*., 252 (2005) 1510.
38. T. Zhang, Y. Shao, G. Meng, Y. Li and F. Wang, *Electrochim. Acta*, 52 (2006) 1323.
39. D.D. Macdonald, *J. Nucl. Mate*r., 379 (2008) 24.
40. A. Fattah-Alhosseini, M.S. Joni, *J. Alloys Compd.*, 646 (2015) 685.
41. T. Zhang, Y. Li and F. Wang, *Corros. Sci.*, 48 (2006) 1249.
42. G. Song, A. Atrens, D.S. John, X. Wu and J. Nairn, *Corros. Sci*., 39 (1997) 1981.

© 2018 The Authors. Published by ESG (www.electrochemsci.org). This article is an open access article distributed under the terms and conditions of the Creative Commons Attribution license (http://creativecommons.org/licenses/by/4.0/).